Computerized Medical Imaging and Graphics 45 (2015) 57–62

Contents lists available at ScienceDirect

Computerized Medical Imaging and Graphics

journal homepage: www.elsevier.com/locate/compmedimag

Intravascular ultrasonic–photoacoustic (IVUP) endoscope with 2.2-mm diameter catheter for medical imaging

Nhat Quang Bui[a], Kyu Kyu Hlaing[a], Van Phuc Nguyen[a], Trung Hau Nguyen[a], Yun-Ok Oh[a], Xiao Feng Fan[a], Yong Wook Lee[a,b], Seung Yun Nam[c], Hyun Wook Kang[a,c], Junghwan Oh[a,c,*]

[a] Interdisciplinary Program of Marine-Bio, Electrical & Mechanical Engineering, Pukyong National University, Busan, South Korea
[b] School of Electrical Engineering, Pukyong National University, Busan, South Korea
[c] Department of Biomedical Engineering, Pukyong National University, Busan, South Korea

ARTICLE INFO

Article history:
Received 21 January 2015
Received in revised form 11 June 2015
Accepted 13 July 2015

Keywords:
Intravascular ultrasound imaging
Intravascular photoacoustic imaging
Imaging endoscope
Indocyanine green
Combined imaging
3D reconstruction

ABSTRACT

Intravascular ultrasound (IVUS) imaging is extremely important for detection and characterization of high-risk atherosclerotic plaques as well as gastrointestinal diseases. Recently, intravascular photoacoustic (IVPA) imaging has been used to differentiate the composition of biological tissues with high optical contrast and ultrasonic resolution. The combination of these imaging techniques could provide morphological information and molecular screening to characterize abnormal tissues, which would help physicians to ensure vital therapeutic value and prognostic significance for patients before commencing therapy. In this study, integration of a high-frequency IVUS imaging catheter (45 MHz, single-element, unfocused, 0.7 mm in diameter) with a multi-mode optical fiber (0.6 mm in core diameter, 0.22 NA), an integrated intravascular ultrasonic–photoacoustic (IVUP) imaging catheter, was developed to provide spatial and functional information on light distribution in a turbid sample. Simultaneously, IVUS imaging was co-registered to IVPA imaging to construct 3D volumetric sample images. In a phantom study, a polyvinyl alcohol (PVA) tissue-mimicking arterial vessel phantom with indocyanine green (ICG) and methylene blue (MB) inclusion was used to demonstrate the feasibility of mapping the biological dyes, which are used in cardiovascular and cancer diagnostics. For the *ex vivo* study, an excised sample of pig intestine with ICG was utilized to target the biomarkers present in the gastrointestinal tumors or the atherosclerotic plaques with the proposed hybrid technique. The results indicated that IVUP endoscope with the 2.2-mm diameter catheter could be a useful tool for medical imaging.

1. Introduction

Photoacoustic imaging (PAI) is based on the optoacoustic effects that result from the formation of acoustic waves due to light absorption in the sample. In this technique, nanosecond laser pulses are typically employed to irradiate biological tissues. Through the conversion of the absorbed light energy into heat, the acoustic waves can be generated within the irradiated volume following the transient thermoelastic expansion of the tissues. These acoustic waves can be identified and collected to reconstruct a photoacoustic image of the spatial distribution of light absorbers from the tissue compositions by using an ultrasound transducer. Therefore, PAI effectively combines the contrast of optical imaging techniques with the penetration depth and the resolution of ultrasound imaging [1–6].

Atherosclerosis is one of the major causes of death in cardiovascular diseases and is caused by a plaque building up in the inner lining of a medium or large artery. The identifying characteristics of a high risk plaques consist the presence of a thin fibrous collagen-rich cap, a large lipid-rich pool, increased plaque inflammation due to dense macrophage activity, hemorrhage and calcification caused by a broken vasa vasorum [7,8]. Gradually building up of a plaque or thickening of the luminal wall of the artery causes decreased the flow of oxygen-rich blood to the tissues, vital organs and extremities. However, new studies have discovered that the structure and composition of the atherosclerotic lesion, rather than the degree of luminal narrowing, are presently considered as the most important decisive factors for acute clinical events [7]. Recently, intravascular photoacoustic (IVPA) imaging has demonstrated many advantages in atherosclerotic plaque detection. It is possible to differentiate

* Corresponding author at: Department of Biomedical Engineering, Pukyong National University, 45 Yongso-ro, Nam-gu, Busan 608-737, South Korea. Tel.: +82 51 629 5771.
E-mail address: jungoh@pknu.ac.kr (J. Oh).

http://dx.doi.org/10.1016/j.compmedimag.2015.07.008
0895-6111/

atherosclerosis based on the structural and functional composition of the plaque by analyzing the multi-wavelength photoacoustic responses of the vessel wall [3,6,9].

During the establishment of atherosclerotic plaques, a variety of biomarkers are present [3]. The accurate detection and characterization of certain biomarkers can ensure vital therapeutic value and prognostic significance for patients diagnosed with atherosclerosis at an early stage while it is asymptomatic. Various contrast agents, such as methylene blue (MB) [10] and gold nanoparticles [3,11], can be used in PAI because of their high optical absorption coefficients. In addition, these contrast agents can be conjugated with a number of antibodies to target biomarkers of interest. However, the MB dye can induce not only chemical mastitis but also photodamage under strong illumination [12]. Furthermore, for clinical applications, gold nanoparticles have not yet been approved by the U.S. Food and Drug Administration [12]. Indocyanine green (ICG, C43H47N2O6S2Na, molecular weight 775 Da), a cyanine dye with infrared absorbing properties, is approved by the Food and Drug Administration for determining human cardiac output, hepatic function, liver blood flow and ophthalmic angiography [13–17]. ICG can be used as a contrast agent for PAI with its absorption maximum of 785 nm in aqueous solutions, and red shifts to 805 nm in blood. After injection, ICG is rapidly metabolized in the liver, and then only excreted via the liver and bile ducts. Importantly, ICG can identify certain cellular and molecular objects involved in atherosclerosis. For instance, ICG has the ability to bind both high-density and low-density lipoproteins, relevant to the characteristics of its lipophilic [18]. In fact, ICG could enable in vivo detection of inflamed atheroma, lipid-rich, human macrophages and human atherosclerosis [19–21].

In the last few years, several IVPA imaging systems have become available for imaging atherosclerosis [2–5]. For example, in the first-generation IVPA systems, the light was delivered from outside of the samples, which were rotated by a motor, while a IVUS transducer was inserted into the lumen for both photoacoustic and reflected ultrasound detections [2,3]. Such designs seem impractical for *in-vivo* imaging in humans due to the external laser irradiation and sample rotation. Subsequently, to enable IVPA imaging in reality, a number of different IVPA system designs, which could perform both of photoacoustic excitation and ultrasound detection inside the samples by integrating a multi-mode optical fiber (MOF) and a high-frequency IVUS into a single catheter, were successfully applied to image the aorta of a rabbit *in vivo* [4,5]. Recently, a combination of a single-mode optical fiber, a high-frequency IVUS transducer and an optical-electric rotary joint was proposed and developed to conduct three-dimensional (3D) volumetric photoacoustic and ultrasound imaging [6]. In general, these techniques seem to be limited in providing the total structure information of the samples due to the scanning mechanism [4,5] or the complicated and costly fabrication process [6]. However, initial experiments using these systems have contributed significantly to physicians' understanding of high-risk plaques and give a demonstration of the prospective of IVPA for determining various components of atherosclerotic plaques.

Here, we present a practical, portable, and cost-effective IVUP endoscope by integrating an IVUS imaging catheter with a custom-made MOF to perform simultaneous IVUS and IVPA imaging in the 3D volumetric of a turbid sample. With a high-frequency transducer, the ultrasound and photoacoustic signals can be resolved with spatial resolutions at the microscopic levels (a few tens of micrometers) [2], as such the resolutions are appropriate for detection of vulnerable plaques [3]. To demonstrate the feasibility of the custom-designed IVUP endoscope, the IVPA and IVUS images of a tissue-mimicking arterial phantom with ICG and MB inclusions are presented to compare the axial and lateral resolutions. In order to improve the ability of the imaging system to discriminate between different compositions based on optical contrast, the co-registered IVPA and IVUS images are shown. The IVUP imaging of an excised pig intestine was also performed to demonstrate the feasibility of the IVUP imaging system in *ex vivo* clinical applications.

2. Experimental methods

2.1. IVUP imaging system

Fig. 1 illustrates a design for an IVUP endoscope system. The key components of our system are a tunable optical parametric oscillator (OPO) laser system pumped by a Q-switched pulsed Nd:YAG laser source, a single-element high-frequency IVUS transducer, a MOF, data acquisition (DAQ) system, and a mechanical scanning stage. For the IVPA imaging, a 532 nm pump source Q-switched pulsed Nd:YAG laser operating at a 10 Hz repetition rate (Surelite III, Continuum, San Jose, CA, USA) was used with a 650–1064 nm wavelength range and a 3–5 ns pulse width using the tunable OPO (Surelite OPO Plus, San Jose, CA, USA). The pumping light was rejected with a 665 nm long-pass colored glass filter (CGF) (FGL665S, Thorlabs, Newton, NJ, USA), and the output laser beam was coupled to a MOF (0.22 numerical aperture [NA], 600 μm core diameter, BFL48-600, Thorlabs) with a plano-convex lens (PCL) (50 mm in focal length, LA1225-B, Thorlabs). The input end of the MOF was fixed to a fiber coupler that could rotate and constantly maintain the MOF at the focus point of the PCL by using two ball bearings. To irradiate the sample that was placed parallel to the imaging catheter, the output end of the MOF was chamfered at an angle of 38 degrees, sealed with a glass cap of 0.9 mm in outer diameter and integrated with a 45-MHz IVUS transducer (Revolution® 45 MHz catheter, Volcano, San Diego, CA, USA) with element size of approximately 0.5 mm to form an IVUP catheter (Fig. 2).

Depending on the size of the samples, the ultrasonic and laser beams must be fairly aligned to detect the strongest photoacoustic signals. Therefore, to facilitate the alignment of the ultrasonic and laser beams, the IVUS catheter was divided into two parts: The adjustment part and the guidance part. The first part, which was used to adjust and fix the IVUS transducer and the MOF to obtain the maximum received signals easily during the scanning process, could rotate both the IVUS transducer and the MOF by an angle of up to $\pm 10^{\circ}$ (respective to the central axis of the catheter) and adjust them by a distance of ±5 mm separately (Fig. 2(a)). The second part had the task of guiding the IVUS transducer and the MOF to the desired scanning positions and protecting the inner surface of the samples from collision with the catheter with a 0.8-mm rounded edge (Fig. 2(b)). The adjustment part was made from ABS (acrylonitrile butadiene styrene, a common thermoplastic polymer) using a 3D printer (the Replicator, Makerbot, Rock Hill, SC, USA). Acrylic glass, a transparent plastic that allows 98% visible light to pass through (with a plate thickness of 3 mm), was used to fabricate the guidance part with a tolerance of 3 μm by using a CNC machine (High-Z S-400/T, CNC-Step, Geldern, Germany). Fig. 2(c) is a digital photograph of the distal end of the catheter under an optical microscope. The custom-made IVUP catheter had a maximum outer diameter of 2.2 mm, making it highly applicable for in vivo clinical investigations in interventional cardiology.

The IVUP catheter was connected to a step motor-gearbox combo (rotary stage) to perform a B-mode scan by rotating the IVUP catheter 360 degrees (counter clockwise) with respect to the central axis of the catheter. To prevent both the MOF and the IVUS catheter from twisting each other, a rotation in the opposite direction (clockwise) was applied to obtain the next B-mode scan. To achieve a 3D image, a series of B-mode scans were recorded step-by-step by longitudinally scanning the sample via another step motor (translation stage). The output signals from the IVUS

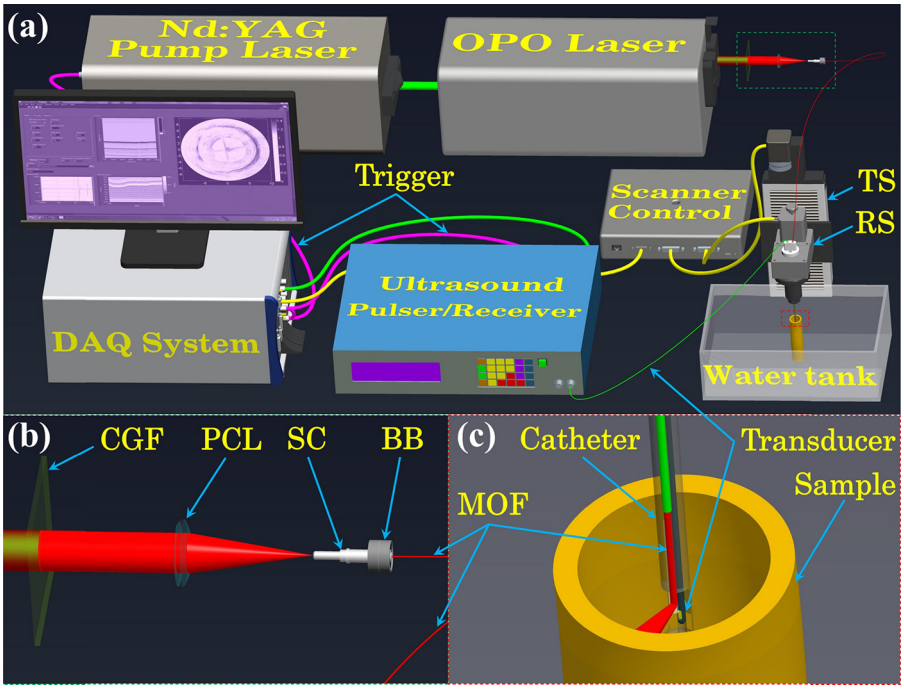

Fig. 1. Illustration of IVUP endoscope system. (a) Overall structure of the experimental setup for IVUP imaging in *ex vivo*. (b) Enlarged view of the green dashed rectangle in (a). (c) Enlarged view of the red dashed rectangle in (a). DAQ: data acquisition; OPO: optical parametric oscillator; TS: translation stage; RS: rotary stage; CGF: color glass filter; PCL: plano-convex lens; SC: SMA connector; BB: ball bearing; MOF: multi-mode optical fiber. (For interpretation of the references to color in this figure legend, the reader is referred to the web version of this article.)

transducer were amplified using an ultrasound pulser/receiver (5900 PR, Olympus, Waltham, MA, USA) before being digitized by a 100-MS/s DAQ card (PXI-5122, National Instruments, Austin, TX, USA) and finally recorded with an embedded controller (NI PXI-1042Q, National Instruments, Austin, TX, USA) with two separate data sets based on the rotary direction of the gearbox. A LabVIEW program was developed to control all the processes mentioned above. The acquired data was band-pass filtered using a linear-phase finite impulse response (FIR) digital filter, processed by the Hilbert transform, and then converted to the Cartesian coordinates to display the 2D cross-sectional and 3D volumetric images of the sample with a custom-developed MATLAB® program.

2.2. *IVUP imaging of a vessel phantom and the tissue samples in* ex vivo

To evaluate the custom-built imaging system, a tissue-mimicking vessel phantom composed of 8% polyvinyl alcohol (PVA, 363146 Aldrich, Sigma-Aldrich, St. Louis, MO, USA) and 0.4% silica powder (S5505 Sigma, Sigma-Aldrich, St. Louis, MO, USA) with

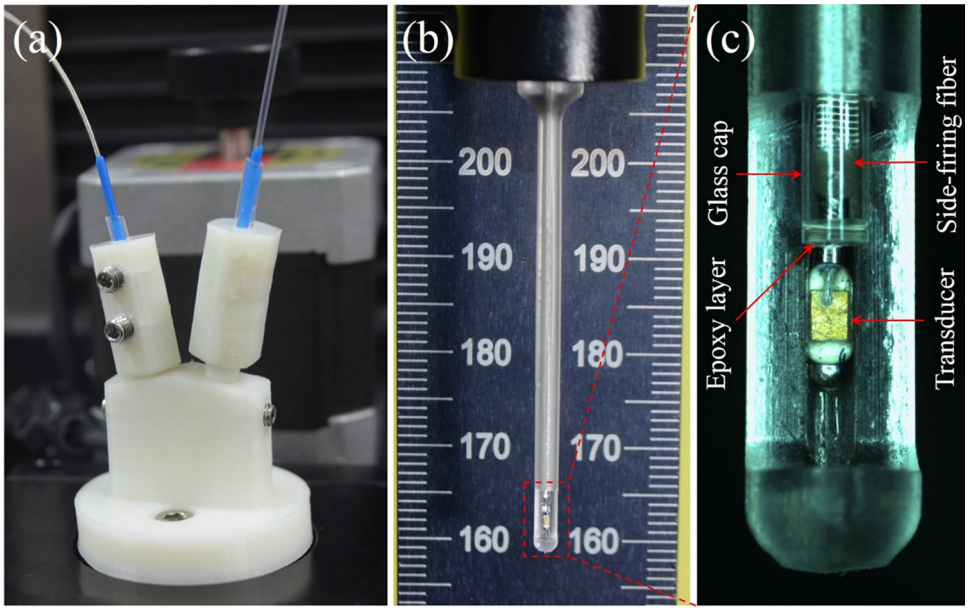

Fig. 2. Fabricated IVUP catheter for experiments. (a) Adjustment part and (b) guidance part of IVUP catheter. (c) Optical microscopic image of the distal end of the guidance part (the red dashed rectangle in (b)). (For interpretation of the references to color in this figure legend, the reader is referred to the web version of this article.)

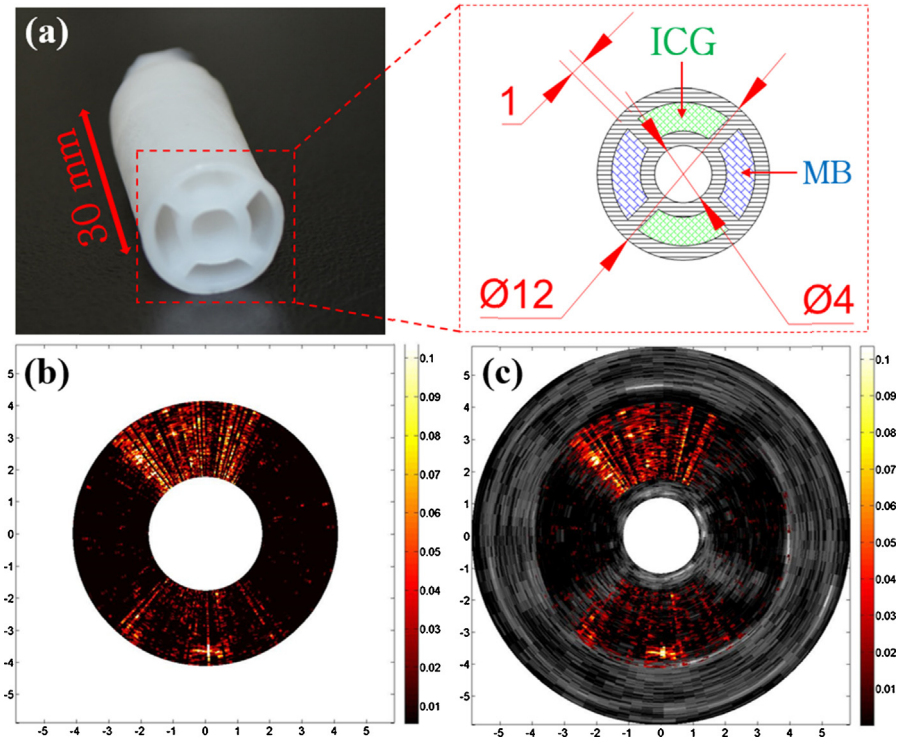

Fig. 3. (a) PVA phantom and the cross section with ICG and MB inclusions. (b) IVPA image. (c) IVUP image. Measurement unit: mm.

ICG and MB inclusions was utilized. PVA was used as the material for the vessel phantoms because of its non-toxic, easy casting, and long-term storage properties, while silica particles (0.2–0.3 μm in diameter) were mixed to the PVA solution to imitate the properties of optical and ultrasound scattering of tissues [22]. The fabrication of a 12-mm outer diameter phantom with 1-mm wall thickness, 4-mm lumen diameter, and four compartments is shown in Fig. 3(a). ICG and MB, the biological dyes used in medical diagnostics, were mixed with degassed water at concentrations of 65 μM and 10 μM, respectively; before being injected alternately into the compartments. The optical absorption coefficient of MB and ICG increases toward the near infrared wavelength range, with local maxima of 677 and 785 nm, respectively [23,24]. To conduct the experiment, the IVUP catheter was put in the lumen of the phantom, which was filled with degassed water to remove artifacts during experiments. The IVUP scans were produced by mechanically rotating the catheter. The setup of the imaging system is shown in Fig. 1.

IVUP imaging studies also were performed of the *ex vivo* samples injected with ICG to target the biomarkers present in the atherosclerotic plaques. The purpose of this study was to demonstrate the feasibility of ICG detection by using this system on biological tissue. Moreover, we targeted a working distance of 0–10 mm from the outer surface of the catheter in designing the endoscope to noninvasively image gastrointestinal diseases, such as colorectal and Barrett's esophagus cancers, which originate from the epithelial cells lining the lumen of the colon of the gastrointestinal tract [5]. Therefore, a section of the intestine with a thickness of 2 mm was extracted from a healthy pig and saved in formalin before conducting the experiment. The PVA vessel phantom with diameter of 12 mm was embedded in the lumen of pig intestine to form the tubular sample before injected with a solution of ICG in water. Similar to the phantom studies, the IVUP imaging catheter was placed in the lumen of the phantom, which was positioned in the water tank and rotated by a stepper motor (rotary stage) to perform the IVUS and IVPA imaging simultaneously.

3. Results

The structure and the cross section of cylindrical the PVA phantom containing four compartments are shown in Fig. 3(a). A 65-μM solution of ICG in water was injected into two of the compartments of the phantom. The remaining two compartments were filled with 10-μM solution of MB in water. The results of the IVPA and IVUP imaging of the vessel mimicking phantom with ICG and MB inclusions are presented in Fig. 3(b) and (c), respectively. Both images are displayed over a 12-mm field of view. To perform the IVUP imaging, 300 ultrasonic and photoacoustic beams, which required a scanning time of 30 s due to the 10-Hz repetition rate of the laser source, were used. A 785-nm optical wavelength was used as the peak absorption of the ICG. In the results, only two ICG filled compartments could be seen, while the other two could not be detected clearly. The reason for this is that the absorption of the individual MB at the 785 nm wavelength was fairly low. If imaged at a 677 nm wavelength, both the ICG and MB would be seen according to their optical absorption properties.

As expected, photoacoustic imaging could not depict the structure of the phantom (Fig. 3(b)). In contrast to the IVPA image, the IVUS image (Fig. 4(a)) plainly shows the structure of the pig intestine with a PVA phantom placed in the lumen. The results indicated that although the biological tissue was placed behind the vessel mimicking phantom (compared with the catheter), IVUS can image the biological tissue with a contrast higher than that of the phantom. The reason is that, the silica particles, which determine the contrast of the ultrasound image, used in our phantom were only 0.2–0.3 μm in diameter while the cell size is ~1–100 μm. However, the IVUS image could not detect the presence of the ICG injected due to a lack of acoustic contrast, whereas the IVUP image (Fig. 4(b)) showed both the position and distribution of the ICG inclusion in the pig intestine. High amplitude photoacoustic signals were detected at the injected areas with a small amount (~0.5 ml) of 6.5-μM solution of ICG in water when performing the IVUP imaging at 785-nm wavelength.

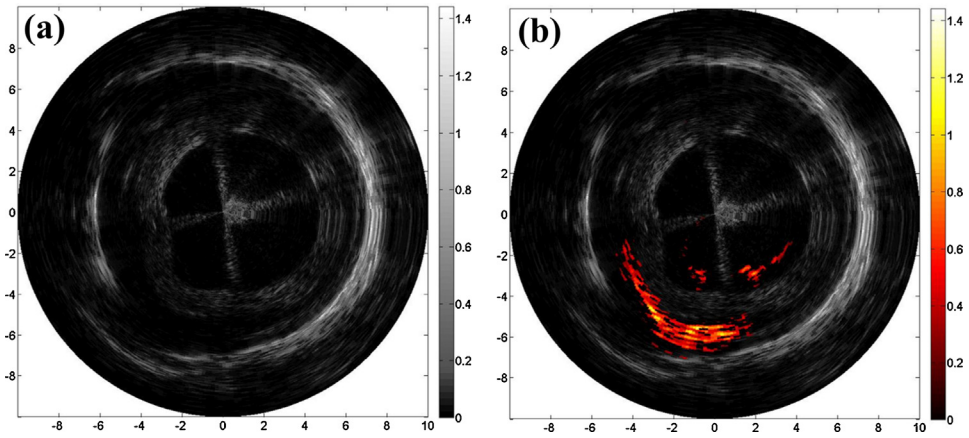

Fig. 4. Pig intestine with ICG injected. (a) IVUS image. (b) IVUP image. Measurement unit: mm.

To demonstrate the ability of the IVUP system to image the distributed inclusion in the sample, a series of 50 B-scans with a step size of 100 μm were performed in the pig intestine injected with ICG. Fig. 5 shows the reconstruction of the 3D IVUP image of the sample from a pullback sequence covering a 5-mm long cylindrical volume with a 20-mm diameter. The left panel shows the volume of $20 \times 20 \times 5$ mm in the Cartesian coordinate system with the ultrasound image in the gray-scale and photoacoustic image in the HSV (Hue-Saturation-Value) color-space. The right panel represents the HSV color-bar of photoacoustic image. The volume-rendered IVUP image shows the ICG solution injected at the interface between tissue and the phantom, and inside two compartments of the phantom.

In all of the experiments, the power of laser irradiation was set at 0.42 mW. Because the laser source operated at a 10 Hz repetition rate, a pulse energy was 0.042 mJ. With a chamfer angle of 38 degrees, the surface area of the output end of the MOF was 0.46 mm^2. According to the NA of 0.22, the fiber had a maximum acceptance angle in water of 9.5 degrees. Since the center axis of the MOF is located at a distance of 0.84 mm from the outer surface of the catheter, the intensity of laser pulse energy incident on the sample at the outer surface of the catheter is maintained below a threshold of 9 mJ/cm^2 during the entire experiment. Consequently, the laser fluence used in our experiment did not exceed the ANSI safety limit (30 W/cm^2) for skin surface exposure at the selected wavelength.

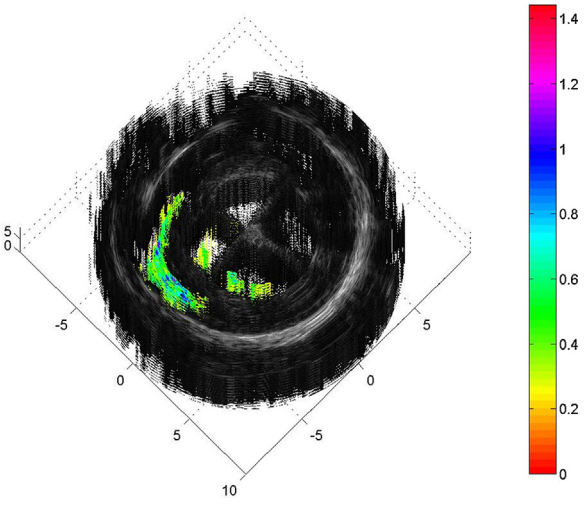

Fig. 5. 3D volumetric IVUP image of pig intestine injected with ICG solution. Measurement unit: mm.

4. Conclusion

IVUP imaging provides a way to visualize the spatial and functional information on light distribution in a atherosclerotic lesions as well as gastrointestinal tumors. We successfully accomplished a 2.2-mm diameter IVUP endoscope, and demonstrated its potential application for mapping the biological dyes in *ex vivo*. The results of this study indicated that the IVUP endoscope could produce the IVUP images of internal organs, detect and localize certain biomarkers in the gastrointestinal tumors or the atherosclerotic plaques based on both their structure and functional composition. Further studies will be conducted with a normal pig aorta to demonstrate the applicability of the IVUP endoscope to interventional cardiology. According to the ability to be adjusted of the catheter, the IVUP endoscope system could be perform on the sample up to 20 mm in diameter. Importantly, by changing the guidance part of IVUP catheter to a flexible one, the feasibility of *in vivo* studies of IVUP endoscope system may be implemented.

Acknowledgments

This research was supported by a grant from Marine Biotechnology Program (20150220) funded by Ministry of Oceans and Fisheries, Republic of Korea.

References

[1] De Montigny E. Photoacoustic tomography: principles and applications. OCIS; 2011.
[2] Sethuraman S, Aglyamov SR, Amirian JH, Smalling RW, Emelianov SY. Intravascular photoacoustic imaging using an IVUS imaging catheter. IEEE Trans Ultrason Ferroelectr Freq Control 2007;54(5):978–86.
[3] Wang B, Su JL, Karpiouk AB, Sokolov KV, Smalling RW, Emelianov SY. Intravascular photoacoustic imaging. IEEE J Sel Top Quantum Electron 2010;16(3):588–99.
[4] Karpiouk AB, Wang B, Amirian J, Smalling RW, Emelianov SY. Feasibility of in vivo intravascular photoacoustic imaging using integrated ultrasound and photoacoustic imaging catheter. J Biomed Opt 2012;17(9):0960081–6.
[5] Yang J-M, Chen R, Favazza C, Yao J, Li C, Hu Z, et al. A 2.5-mm diameter probe for photoacoustic and ultrasonic endoscopy. Opt Express 2012;20(21):23944–53.
[6] Bai X, Gong X, Hau W, Lin R, Zheng J, Liu C, et al. Intravascular optical-resolution photoacoustic tomography with a 1.1 mm diameter catheter. PLoS ONE 2014;9(3):e92463.
[7] Naghavi M, Libby P, Falk E, Casscells SW, Litovsky S, Rumberger J, et al. From vulnerable plaque to vulnerable patient a call for new definitions and risk assessment strategies: Part I. Circulation 2003;108(14):1664–72.
[8] Virmani R, Kolodgie FD, Burke AP, Farb A, Schwartz SM. Lessons from sudden coronary death a comprehensive morphological classification scheme for atherosclerotic lesions. Arterioscler Thromb Vasc Biol 2000;20(5):1262–75.
[9] Jansen K, Wu M, van der Steen AF, van Soest G. Lipid detection in atherosclerotic human coronaries by spectroscopic intravascular photoacoustic imaging. Opt Express 2013;21(18):21472–84.

[10] Song KH, Margenthaler JA, Wang LV, Stein EW. Noninvasive photoacoustic identification of sentinel lymph nodes containing methylene blue in vivo in a rat model. J Biomed Opt 2008;13(5), 054033-054033-054036.
[11] Conjusteau A, Ermilov SA, Lapotko D, Liao H, Hafner J, Eghtedari M, et al. Metallic nanoparticles as optoacoustic contrast agents for medical imaging. In: Biomedical optics 2006: 2006. International Society for Optics and Photonics; 2006, 60860K-60860K-60869.
[12] Kim C, Song KH, Gao F, Wang LV. Sentinel lymph nodes and lymphatic vessels: noninvasive dual-modality in vivo mapping by using indocyanine green in rats—volumetric spectroscopic photoacoustic imaging and planar fluorescence imaging 1. Radiology 2010;255(2):442–50.
[13] Fox I, Brooker L, Heseltine D, Essex H, Wood E. A tricarbocyanine dye for continuous recording of dilution curves in whole blood independent of variations in blood oxygen saturation. In: Proceedings of the Staff Meetings. 1957. p. 478.
[14] Caesar J, Shaldon S, Chiandussi Le, Guevara L, Sherlock S. The use of indocyanine green in the measurement of hepatic blood flow and as a test of hepatic function. Clin Sci 1961;21:43.
[15] Desmettre T, Devoisselle J, Mordon S. Fluorescence properties and metabolic features of indocyanine green (ICG) as related to angiography. Surv Ophthalmol 2000;45(1):15–27.
[16] Benson RC, Kues HA. Fluorescence properties of indocyanine green as related to angiography. Phys Med Biol 1978;23(1):159.
[17] Flower RW. Evolution of indocyanine green dye choroidal angiography. Opt Eng 1995;34(3):727–36.
[18] Yoneya S, Saito T, Komatsu Y, Koyama I, Takahashi K, Duvoll-Young J. Binding properties of indocyanine green in human blood. Invest Ophthalmol Vis Sci 1998;39(7):1286–90.
[19] Vinegoni C, Botnaru I, Aikawa E, Calfon MA, Iwamoto Y, Folco EJ, et al. Indocyanine green enables near-infrared fluorescence imaging of lipid-rich, inflamed atherosclerotic plaques. Sci Transl Med 2011;3(84):84ra45, http://dx.doi.org/10.1126/scitranslmed.3001577. http://stm.sciencemag.org/content/3/84/84ra45
[20] Stanga PE, Lim JI, Hamilton P. Indocyanine green angiography in chorioretinal diseases: indications and interpretation: an evidence-based update. Ophthalmology 2003;110(1):15–21.
[21] Fischer T, Gemeinhardt I, Wagner S, Stieglitz DV, Schnorr J, Hermann K-GA, et al. Assessment of unspecific near-infrared dyes in laser-induced fluorescence imaging of experimental arthritis. Acad Radiol 2006;13(1):4–13.
[22] Kharine A, Manohar S, Seeton R, Kolkman RG, Bolt RA, Steenbergen W, et al. Poly (vinyl alcohol) gels for use as tissue phantoms in photoacoustic mammography. Phys Med Biol 2003;48(3):357.
[23] Oregon Medical Laser Center. Optical absorption of methylene blue; 2014. ⟨http://omlc.org/spectra/mb/index.html⟩ (Dec 10, 2014).
[24] Landsman M, Kwant G, Mook G, Zijlstra W:. Light-absorbing properties, stability, and spectral stabilization of indocyanine green. J Appl Physiol 1976;40(4):575–83.